International Journal of Earth Sciences
https://doi.org/10.1007/s00531-019-01751-5

ORIGINAL PAPER

Late Cretaceous exhumation and uplift of the Harz Mountains, Germany: a multi-method thermochronological approach

Hilmar von Eynatten[1] · István Dunkl[1] · Manfred Brix[2] · Veit-Enno Hoffmann[1] · Matthias Raab[3] · Stuart Nigel Thomson[4] · Barry Kohn[3]

Received: 18 February 2019 / Accepted: 29 June 2019

Abstract

The Harz Mountains represent one of the most prominent surface expressions of Late Cretaceous intraplate shortening in Central Europe. We present a comprehensive low-temperature thermochronological data set (zircon and apatite, fission track and [U–Th]/He) covering the exhumed Paleozoic basement of the Harz Mountains and the adjacent Kyffhäuser block, as well as Lower Triassic sedimentary rocks of the western and southern rim of the Harz Mountains. Integration of results with sedimentological data from the syntectonic Late Cretaceous Subhercynian Basin allows for a detailed reconstruction of the timing of uplift and erosion of the Harz Mountains. The data reveal that (i) tectonic reorganization and initial exhumation started at around 90 Ma, (ii) uplift and emergence caused erosion of the Mesozoic sedimentary cover between 86–85 Ma and 83–82 Ma, and (iii) erosion of at least 3–4 km of underlying Paleozoic rocks followed and continued into the Paleogene. The thickness of removed overburden amounts to at least 6 km, and most erosion occurred in Santonian to Campanian time at minimum rates of ~ 0.5 km/Myr. The southwestern rim of the Harz has exhumed slower over a longer period of time, and may record a phase of Late Cretaceous, syntectonic sediment accumulation.

Keywords Thermochronology · Fission track · (U–Th)/He · Late Cretaceous · Intraplate stress · Subhercynian Cretaceous Basin · Central Europe

Introduction

Widespread intraplate compressional stresses affected Central Europe in Late Mesozoic to Early Cenozoic time and generated numerous basement uplifts and inverted sedimentary basins (e.g. Ziegler et al. 1995; Kley and Voigt 2008). The basement uplifts are distributed over a large area extending roughly west to east along the southern margin of the Central European Basin System (cf. Littke et al. 2008) from the Ardennes in Belgium (western Rhenish Massif) to southern Poland and Czech Republic (e.g. Karkonosze Mountains; Fig. 1). The major phase of uplift and basin inversion is generally assigned to the Late Cretaceous. However, earlier onset of exhumation and uplift and continuation of inversion and exhumation into the Paleogene has been proposed for certain areas and structures (e.g. Kockel 2003; Karg et al. 2005).

Among the basement uplifts, the Harz Mountains in central Germany are considered unique because of (i) a well-exposed basement structure slightly tilted towards SSW, (ii) a well-defined WNW striking northern boundary fault zone, and (iii) an intensely explored and well-exposed syntectonic sedimentary basin north of the fault zone (Subhercynian Cretaceous Basin). The sedimentary record within the basin and a high-resolution biostratigraphy allows for a detailed reconstruction of unconformities (Voigt et al. 2004), facies

Electronic supplementary material The online version of this article (https://doi.org/10.1007/s00531-019-01751-5) contains supplementary material, which is available to authorized users.

✉ Hilmar von Eynatten
heynatt@gwdg.de

1 Geoscience Center, Department of Sedimentology and Environmental Geology, University of Göttingen, Goldschmidtstrasse 3, 37077 Göttingen, Germany

2 Institute of Geology, Mineralogy, and Geophysics, Faculty of Geosciences, Ruhr University Bochum, Universitätsstrasse 150, 44801 Bochum, Germany

3 School of Earth Sciences, University of Melbourne, Melbourne, Victoria 3010, Australia

4 Department of Geosciences, University of Arizona, Tucson, AZ 85721, USA

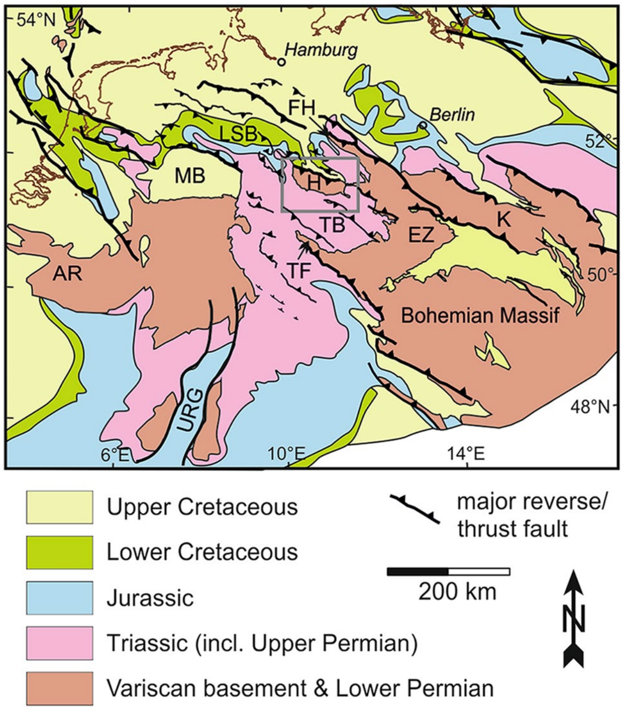

Fig. 1 Pre-Tertiary geologic sketch indicating position of the Harz Mountains within the Central European array of Variscan basement highs. Note frequent juxtaposition of basement highs and Late Cretaceous sedimentary basins along NW–SE trending reverse or thrust faults (modified after Ziegler 1990; Kley and Voigt 2008). Grey box indicates position of Fig. 2. *AR* Ardennes, *EZ* Erzgebirge, *FH* Flechtingen High, *H* Harz Mountains, *K* Karkonosze Mountains, *LSB* Lower Saxony Basin, *MB* Münsterland Basin, *TB* Thuringian Basin, *TF* Thuringian Forest, *URG* Upper Rhine Graben

distribution (Voigt et al. 2006) and sediment provenance (von Eynatten et al. 2008). No such in-depth reconstruction of exhumation and uplift based on the tectono-sedimentary evolution of the syntectonic basin has yet been carried out at this level of detail for any of the other Central European uplifted basement blocks.

This reconstruction of uplift of the Harz basement block is, however, based largely on observations from syntectonic sedimentary rocks, with scarce supporting data on the thermal evolution and exhumation of the uplifted basement massif itself. This paper fills this gap by evaluating timing and rates of exhumation of the Harz Mountains using a multi-method thermochronological approach that includes apatite and zircon fission track analysis (AFT and ZFT, respectively) as well as apatite and zircon (U–Th)/He analysis (AHe and ZHe, respectively). The new results allow for (i) precise constraints on the timing and rates of cooling and exhumation of the Harz Mountains, (ii) combining of results from thermochronology with the adjacent sedimentary record, and (iii) comparison of the exhumation of the Harz Mountains with its southwestern foreland.

Geological setting

The Harz Mountains in central Germany represent an uplifted and deeply eroded block of Paleozoic rocks, which constitutes one of the most prominent surface expressions of Late Cretaceous uplift and inversion structures in Central Europe. The basement rocks are mainly composed of very low-grade metasedimentary rocks and minor metabasalts, which have been overprinted and folded during the Variscan orogeny and are intruded by late Variscan granite bodies (Kley et al. 2008; McCann 2008; Fig. 2). The Harz Mountains form a WNW-ESE elongated basement block of approximately 90 km length and 30 km width, surrounded by Upper Permian (Zechstein) and Mesozoic rocks. Mean elevation varies between 500 and 700 m a.s.l., slightly decreasing towards ESE. The highest peak in the central part (Brocken) is at 1141 m a.s.l. while the lowlands surrounding the Harz Mountains range between 150 and 250 m a.s.l.

The Harz Mountains are bordered to the north by a WNW striking fault zone (Harz Northern Boundary Fault, HNBF), which separates the uplifted basement block from the adjacent syntectonic basin to the north (Subhercynian Cretaceous Basin, SCB). A zone of steeply inclined Upper Permian to Cretaceous rocks is sandwiched between the HNBF and the Late Cretaceous basin fill (Fig. 2), demonstrating flexural deformation due to the formation of a fault propagation fold (Voigt et al. 2004). The HNBF itself is a Late Cretaceous reverse fault, dipping between 30° to 60° towards (S)SW with a minimum horizontal shortening of about 4 km and minimum vertical displacement of 3 km as inferred from cross sections (DEKORP-Basin Research Group 1999; Franzke et al. 2004). Taking into account (i) preliminary AFT data which suggest Late Cretaceous removal of 3–5 km of overburden from the present-day surface of the Harz (Thomson et al. 1997) and (ii) > 2 km thickness of Late Cretaceous strata adjacent to the fault zone (see below), the relative vertical displacement across the HNBF amounts to at least 7 km (Kley et al. 2008). This number is consistent with geometrical considerations indicating 6 km of vertical throw (e.g. Flick 1986), and exceeds by orders of magnitude possible vertical offsets at the southern, eastern, and western boundaries of the Harz Mountains. The contrast between NNE-directed thrusting and huge vertical offset in the north and small to zero offset in the south along with paleo-stress data (Franzke et al. 2007) and many other arguments (summarized in Voigt et al. 2009) call for the interpretation of the HNBF as a relatively steep frontal thrust fault in the Paleozoic basement, which was accompanied by flexural folding of the Mesozoic cover rocks during NNE-ward fault propagation. A decrease in fault angle with increasing depth

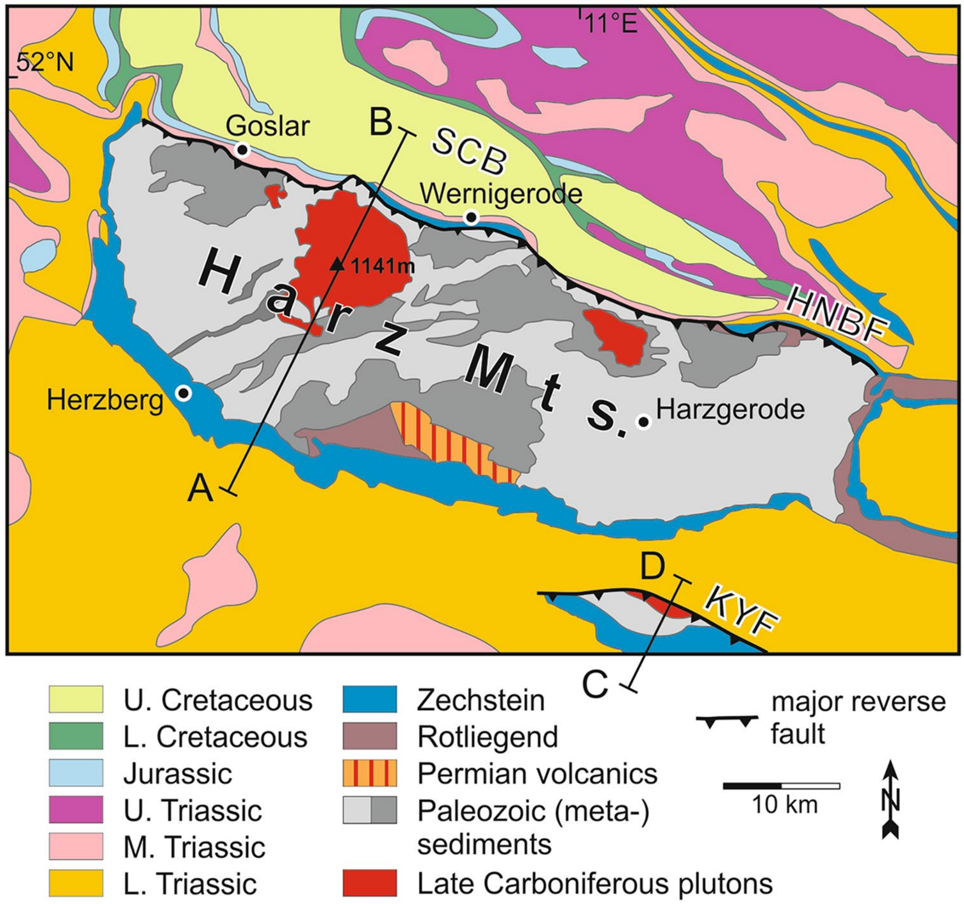

Fig. 2 Pre-Tertiary geological sketch map (simplified from geological map GK 400 Sachsen-Anhalt) of the Harz Mountains and surrounding areas including Kyffhäuser high (KYF). Note steeply inclined Harz northern boundary thrust fault (HNBF) and adjacent Subherynian Cretaceous Basin (SCB). Between HNBF and SCB steeply dipping Permo–Mesozoic strata mark the trace of a fault propagation fold developed in front of the thrusted Harz Mountains. Plutons are from west to east: Oker (small), Brocken (largest with highest peak at 1141 m a.s.l.), and Ramberg. A to B and C to D denote the traces of the cross sections presented in Fig. 7. Sample locations and codes are not included for reason of readability (see electronic supplementary material)

passing into a horizontal detachment at crustal depths estimated between 12 and 25 km is suggested by deep seismic profiles and kinematic reconstructions (DEKORP-Basin Research Group 1999; Tanner and Krawczyk 2017).

The Subhercynian Cretaceous Basin is a narrow (~ 15 km) basin extending over ca. 90 km along strike in front of the Harz Mountains (Fig. 2). The basin fill comprises Cenomanian to lower Campanian sedimentary rocks forming a WNW striking wedge-like structure with maximum thicknesses of 2.5–3 km in the southern basin parts immediately north of the HNBF (Voigt et al. 2006). Lithology changes from pelagic-hemipelagic limestones in Cenomanian to Turonian time to dominantly marly deposits in Coniacian to early Campanian time. The latter locally interfinger with sandy intervals, which increase upsection. Several angular unconformities are developed within the basin, especially in the Santonian to early Campanian in the southern basin part. The spatial–temporal distribution of the unconformities suggests the development of a continuously growing fault-propagation fold during that time interval (Voigt et al. 2004). Facies distribution and provenance indicators demonstrate that (i) basin formation initiated in the late Turonian (~ 90 Ma) reflected by increasing thickness and fine-grained siliciclastic input, (ii) from the middle Santonian on (~ 85 Ma) the initial Harz uplift acted as nearby source for coarse-grained detritus, (iii) erosion of the Mesozoic cover of the Harz Mountains peaked at around the Santonian–Campanian transition (84–83 Ma), and (iv) erosion of the Harz Mountains reached the Paleozoic basement by early Campanian time (~ 82 Ma) implying that the 2–3 km thick Mesozoic cover of the Harz Mountains was removed within ~ 3 Myr, i.e. at an average rate of about 1 km/Myr (Voigt et al. 2006; von Eynatten et al. 2008).

The stress field and the external forces controlling Late Cretaceous intraplate compression in Central Europe has been a matter of debate for decades (e.g. Stackebrandt and Franzke 1989; Ziegler 1987; Ziegler et al. 1995; Marotta et al. 2001; Kley and Voigt 2008). NNE-directed thrusting in Central Europe is now widely accepted as having been caused by a major change in Africa's motion relative to Europe, i.e. from SE directed sinistral transform motion to NE directed convergence. This change occurred between 90 and 84 Ma, matching the timing observed for uplift of the Harz Mountains, deformation in the adjacent Subhercynian Cretaceous Basin, and related structures in Central Europe (Kley and Voigt 2008).

Sampling strategy and methods

Sampling was primarily intended to spatially cover the entire Harz Mountains. However, this was partly hampered by difficulties in finding appropriate lithologies because most of the siliciclastic (meta)sedimentary rocks are pelites and/or did not yield appropriate apatite required for low temperature thermochronology. The most suitable samples cluster at the major granitoid bodies (from E to W Ramberg, Brocken, and Oker plutons; Fig. 2), complemented by a few greywackes, two rhyolites and one gneiss (Ecker gneiss). For a detailed sample list and sample location map see supplementary material. Besides basement rocks of the Harz Mountains, we sampled (i) a Paleozoic greywacke at the southernmost tip of the Harz, (ii) several Lower Triassic sandstones ("Buntsandstein") from the western and southern rim of the Harz, and (iii) granite and Carboniferous sandstone from the Kyffhäuser block to evaluate the potential contrast between the Harz basement block and its close surroundings (for sample location map see supplementary material). The Kyffhäuser is a small block of exhumed Variscan basement ~ 10 km south of the Harz Mountains covered by Upper Carboniferous to Permian sedimentary rocks and separated from Mesozoic rocks to the north by a steep reverse fault, which strikes similar to the HNBF (Fig. 2). Two sandstone samples from the Upper Cretaceous Subhercynian Basin were also collected for ZFT analysis.

Apatite and zircon crystals were separated by crushing, sieving, gravity and magnetic separation techniques. AFT analysis was conducted on almost all samples, while ZFT, ZHe and AHe analyses were concentrated in the Brocken area because this is the only region within the Harz Mountains where a potential age-elevation trend might be detectable. Further AHe analyses were performed for the western and southern rim including the Kyffhäuser.

Fission track thermochronology was performed at the fission track laboratories of Ruhr University Bochum, University of Melbourne, and Geoscience Center Göttingen. The external detector method and the zeta age calibration approach were used to determine the fission track age (Gleadow 1981; Hurford and Green 1983; Hurford 1990). Polished apatite grain mounts were etched for 20 s in 5.5 N HNO_3 at 21 °C, while for zircon mounts the eutectic melt of NaOH–KOH at 210 °C was used for 3–6 h (Gleadow et al. 1976). Corning CN standard glasses were used as a dosimeter to monitor the neutron flux. Samples together with age standards (Fish Canyon, Durango, and Tardree rhyolite) were irradiated at the Oregon State University TRIGA reactor in the USA. After irradiation the muscovite external detectors were etched for about 30 min in 40% HF at room temperature in order to reveal the induced tracks. Spontaneous and induced fission tracks were counted dry under 1000× magnification using a Zeiss Axioskop microscope equipped with computer-controlled stage system (Dumitru 1993). Zircon fission tracks were counted in oil immersion under 1250× magnification on a Zeiss Axioplan microscope, using a Lang stage and in-house software. All quoted fission track ages are central ages (Galbraith and Laslett 1993), and the spread of single grain ages was assessed using the dispersion of the central age and Chi-square test (Galbraith 1981). The chlorine content and the etch pit diameter (Dpar) of the apatites were used as control parameter of annealing kinetics (Carlson et al. 1999). At least four, c-axis parallel etch pits per single analyzed grain were measured (Donelick et al. 2005). For each sample, as many horizontal confined track lengths as possible were measured (Gleadow et al. 1986; Green 1981).

For (U–Th)/He thermochronology, single-crystal aliquots were dated at the GÖochron laboratories of the Goecience Center Göttingen, at minimum three grains per sample. Only fissure-free, intact, well-developed crystals were used; euhedral ones were preferred. The shape parameters were determined and recorded by multiple digital photomicrographs. The crystals were wrapped in platinum capsules of ca. 1 × 1 mm size and heated by an infra-red laser. The extracted gas was purified using a SAES Ti–Zr getter at 450 °C. The chemically inert noble gases and a minor amount of remaining gases were then expanded into a Hiden triple-filter quadrupole mass spectrometer equipped with a positive ion counting detector. Crystals were checked for degassing of He by sequential reheating and He measurement. The residual gas is usually around 1–2% after the first extraction in case of zircon crystals and always below 1% in case of apatite crystals. Following degassing, samples were retrieved from the gas extraction line and spiked with calibrated ^{230}Th and ^{233}U solutions. Zircon crystals were extracted from the Pt capsules and dissolved in Teflon vials within pressurized digestion bombs using a mixture of double distilled 48% HF and 65% HNO_3 at 220 °C for 5 days. Apatite crystals were dissolved in pre-spiked 4% HNO_3. The solutions were analysed by isotope dilution method using a Perkin Elmer Elan DRC II ICP-MS with an APEX micro-flow nebulizer. Sm, Zr, Pt and Ca were determined by external calibration. The ejection correction factors (Ft) were determined for the single crystals by a modified algorithm of Farley et al. (1996) using an in-house spreadsheet.

For the modelling of the thermal history we have selected six samples representing different structural blocks, stratigraphic levels and measured ages. HeFTy software (Ketcham 2005). The HeFTy modelling program (Ketcham 2005) requires input data (such as measured AFT age, uncorrected track length distribution, kinetic parameters like Dpar or Cl content, and the AHe age, actinide concentration and diameter of the selected crystals) as well as geological constraints for the time–temperature history. The procedure was operated with the multi-kinetic fission track annealing model of Ketcham et al. (2007) and the diffusion kinetics after Farley (2000). The modelling was performed in 'unsupervised' mode, only the time–temperature constraints were limited to the age of metamorphism, the age of sedimentation and the current annual mean temperature of 6–8 °C. Any other limitations of the potential thermal paths were avoided. Randomly generated thermal histories predict the AFT and AHe ages and track length parameters, and compare them to the measured data. An acceptable fit corresponds to thermal histories representing the t–T paths that give a goodness of fit (GOF) value > 0.05 for both the age and the length distribution (Ketcham 2005). A good fit corresponds to thermal histories with a GOF value > 0.5. The best fit models usually yield GOF values of > 0.9 for AFT and AHe ages and track length parameters. For a comprehensive overview of fission-track methods and their modelling techniques, see Donelick et al. (2005), Ketcham (2005), and Ketcham et al. (2007).

Results

Zircon fission-track data (ZFT)

ZFT data from seven granite samples from the Brocken and Oker plutons show a narrow Triassic age range from 229 to 202 Ma, undistinguishable within error, while a gneiss sample (ECK) from between the two plutons yields 258 Ma (Table 1; Fig. 3). Detrital zircons in Upper Cretaceous sandstones from the SCB yield broad Paleozoic to Triassic ZFT age spectra with Permo–Carboniferous central ages (samples LEH1 and TEU1, 343 and 282 Ma, respectively).

Zircon (U–Th)/He data (ZHe)

Eighteen zircon grains from two samples from different elevations of the Brocken area yield significantly contrasting ZHe mean ages for the low elevation sample (EY40-4, 432 m a.s.l., 103.6 ± 4.3 Ma) and the high elevation sample (EY40-9, 1105 m a.s.l., 150.9 ± 7.7 Ma (Table 2; Fig. 3).

Apatite fission-track data (AFT)

All AFT data passed the Chi-square test except for two sandstone and one granite sample (out of 36 samples; Table 3). Twenty samples from the Harz plutons indicate a very narrow age range from 83 to 73 Ma, undistinguishable within error (Table 3, Fig. 3). No spatial contrasts or elevation trends are observed, which is supported by additional data from six Paleozoic greywacke and rhyolite samples between and south of the plutons yielding ages between 83 and 77 Ma. All these samples show narrow track length distributions with long mean track lengths between 12.7 and 14.1 µm (only samples with number of measured track lengths > 20; see Table 3 and electronic supplement for illustration of track length distributions). Samples from the Kyffhäuser block yield similar ages, although showing a wider range of 95–59 Ma (Fig. 3). In contrast, AFT data measured on mostly Lower Triassic sandstone samples from the western and southern rim of the Harz Mountains indicate significantly older ages of 144–110 Ma along with broader (e.g. V-15, V-126), partly bimodal (e.g., V-13, V-124) track length distributions (Table 3 and electronic supplement).

Table 1 Zircon fission track results obtained on basement and Mesozoic samples from the Harz Mountains and surroundings

Sample	Cryst	Spontaneous		Induced		Dosimeter		$P(\chi^2)$	Disp.	FT age[a]
		RhoS	(Ns)	RhoI	(Ni)	RhoD	(Nd)	(%)		(Ma ± 1 s)
OK 13	16	15.5	(2.518)	2.06	(335)	0.500	(13.771)	24	0.16	213 ± 16
GB	15	15.8	(2.311)	2.16	(331)	0.499	(13.770)	15	0.07	202 ± 13
BR 281 C	8	30.0	(2.607)	3.70	(322)	0.448	(6.181)	9	0.06	213 ± 14
BR 325 B	9	27.8	(1.884)	3.13	(216)	0.448	(6.181)	9	0.04	228 ± 17
BR 327 C	10	32.1	(2.396)	3.65	(272)	0.448	(6.181)	12	0.10	229 ± 17
BR 362 B	20	36.8	(5.188)	4.44	(626)	0.448	(6.681)	33	0.15	215 ± 12
BR 386 B	7	26.0	(1.975)	3.21	(133)	0.448	(6.181)	2	0.00	212 ± 20
ECK	19	24.5	(3.144)	2.36	(303)	0.430	(5.939)	24	0.14	258 ± 18
TEU1	20	18.3	(2.671)	1.68	(246)	0.447	(6.170)	12	0.00	282 ± 19
LEH1	20	18.5	(3.471)	1.60	(301)	0.529	(7.290)	44	0.30	343 ± 32

Track densities (Rho) are as measured ($\times 10^5$ tr/cm^2); number of tracks counted (*N*) shown in brackets

$P(\chi^2)$ probability obtaining Chi-square value for *n* degree of freedom (where *n* no. crystals-1)

Cryst number of dated apatite crystals, *Disp* dispersion, according to Galbraith and Laslett (1993)

[a]Central ages

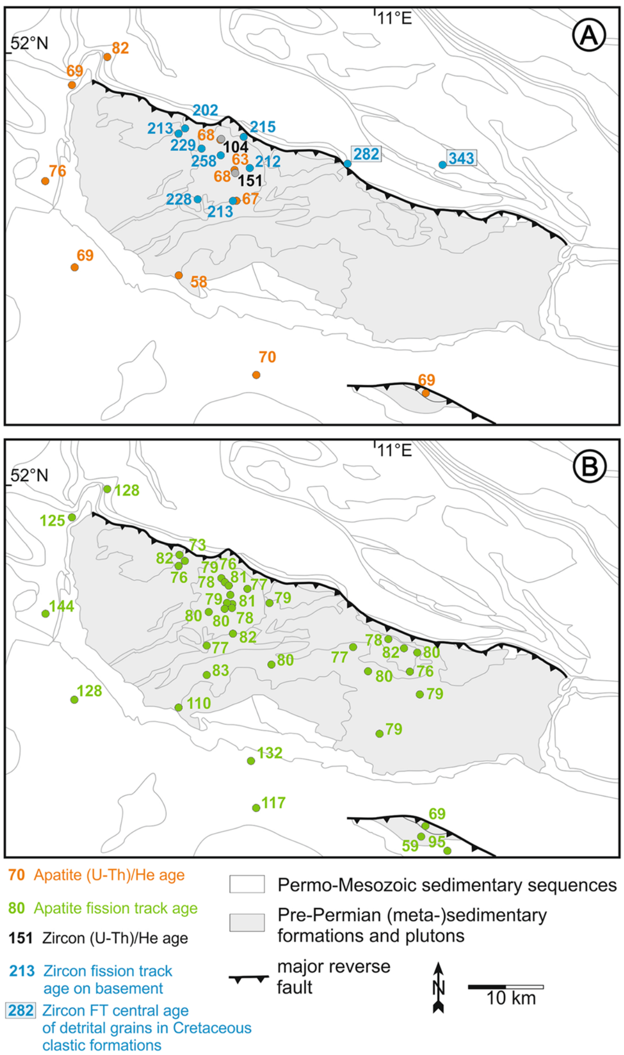

Fig. 3 Spatial distribution of the low-temperature thermochronological mean ages of all dated samples, separated for individual methods: **A** ZFT, ZHe and AHe; **B** AFT. Analytical details are listed in Tables 1, 2, 3 and 4. Further information on sample location including spatial distribution of sample codes can be found in the electronic supplement

Apatite (U–Th)/He data (AHe)

Four samples (3–7 dated grains each) from the Brocken area yield very consistent AHe mean ages between 68 and 63 Ma (EY-samples; Table 3; Fig. 3). The spread within the 24 single-crystal aliquot ages most likely derives from zonation and undetected fluid inclusions even in the best-suited apatite grains. Seven samples with 19 dated apatite grains from the southern and western rim of the Harz and the Kyffhäuser (V-samples) yield similar Late Cretaceous to Paleocene ages although the spread in sample mean ages is larger (82–58 Ma).

Discussion

The Permian to Triassic ZFT ages from the Harz Mountains coincide with ZFT ages from Paleozoic basement units of the wider region, including the Western Bohemian Massif, Flechtingen High, Thuringian Forest and Late Carboniferous rhyodacites of the nearby Halle Volcanic Complex (Fig. 4A, B). These ages are significantly younger than the post-Variscan cooling event and are most likely formed by weak rejuvenation (partial reset) due to Permo–Mesozoic burial heating (e.g., Jacobs and Breitkreuz 2003; Fischer et al. 2012).

ZHe data from the Brocken area show significant contrast between the high and the low elevation samples. The low elevation sample (EY40-4, 432 m a.s.l.) shows, besides a much younger mean age (~ 104 Ma), a distinct and tight youngest age component (5 out of 9 ages between 96 and 90 Ma; Fig. 5; Table 2). In contrast, the high elevation sample (EY40-9, 1105 m a.s.l.) shows scattered Early Jurassic to Early Cretaceous ages with a Late Jurassic mean (~ 151 Ma). This large spread in ages could result from long-lasting burial heating, resulting in different degrees of diffusional loss of helium from the individual zircon crystals, according to their individual size and radiation damage density (e.g. Reiners et al. 2004; Guenthner et al. 2013). Such age dispersion could also result from different degrees of zonation of parent isotopes within crystals or the presence of He-rich inclusions (e.g. Danišík et al. 2017). The pronounced asymmetry of the single-grain ZHe ages from the low elevation sample, however, may indicate incomplete resetting with some memory left from pre-exhumation time, which is typical for samples from the partial retention zone (PRZ). Therefore, the sample mean cannot be taken as meaningful number for reconstructing the thermal evolution. Instead, the mean of the tight youngest age component at 93.6 ± 2.1 Ma is considered relevant for the thermal history. Moreover, this age is concordant with data from the Flechtingen High further to the north with a youngest ZHe age component of ~ 92 Ma (Fischer et al. 2012). The data suggest that the lowest accessible elevation (~ 400 m a.s.l.) of incised valleys in the Brocken granite region represents the level of transition between the totally reset zone and the PRZ of the ZHe thermochronometer before Late Cretaceous exhumation (similar to the low-elevated Flechtingen High). In contrast, the peak level of the Brocken pluton was located within the PRZ at that time. The early Late Cretaceous ZHe ages of the low elevation sample of the Harz Mountains and from the Flechtingen High are similar to Middle to Late Cretaceous ZHe ages observed at significant faults defining the NE-boundary of the Bohemian Massif further east (Danišík et al. 2010, 2012), suggesting roughly synchronous cooling and exhumation of similar magnitude.

Table 2 Zircon (U–Th)/He results obtained on basement samples from the Harz Mountains

Sample	Aliq.	He		U238			Th232			Th/U	eU	Ejection	Uncorr.	Ft-Corr.	2σ	Sample unweighted aver. ± 1 s.e.	
		Vol.	1σ	Mass	1σ	Conc.	Mass	1σ	Conc.			Correct.	He-age	He-age			
		[ncc]	[%]	[ng]	[%]	[µg/g]	[ng]	[%]	[µg/g]	ratio	[µg/g]	(Ft)	[Ma]	[Ma]	[Ma]	[Ma]	[Ma]
EY40-4	#1	14.3	0.3	1.43	1.8	242	0.65	2.4	111	0.46	268	0.78	74.3	95.0	6.9		
	#2	13.2	0.2	1.04	1.8	135	0.58	2.4	75	0.55	153	0.80	91.8	114.5	7.7		
	#3	5.7	0.4	0.61	1.8	129	0.21	2.4	44	0.34	139	0.77	72.1	94.3	7.3		
	#5	11.2	0.3	1.16	1.8	181	0.46	2.4	71	0.40	197	0.78	72.3	92.4	6.7		
	#6	16.2	0.3	1.23	1.8	248	0.60	2.4	120	0.48	276	0.76	96.6	127.0	10.0		
	#7	8.5	1.7	0.96	1.8	212	0.40	2.4	88	0.42	233	0.74	66.5	90.0	8.2		
	#8	15.3	1.6	1.35	1.8	188	0.49	2.4	68	0.36	205	0.79	86.3	109.6	8.6		
	#9	6.9	1.7	0.61	1.8	143	0.26	2.4	61	0.43	157	0.75	85.1	113.8	10.1		
	#10	22.7	1.6	2.23	1.8	255	0.87	2.4	100	0.39	278	0.80	76.7	96.1	7.3	103.6	4.3
EY40-9	#1	37.9	0.3	2.06	1.8	156	1.42	2.4	107	0.69	181	0.82	129.7	158.4	9.9		
	#2	40.4	0.3	2.74	1.8	421	1.40	2.4	214	0.51	471	0.78	108.1	138.3	10.1		
	#3	145.2	0.6	5.64	1.8	882	11.02	2.4	1723	1.95	1286	0.78	144.3	184.6	13.3		
	#5	23.5	1.6	1.67	1.8	202	0.69	2.4	83	0.41	221	0.80	105.3	132.4	10.1		
	#6	48.4	1.6	2.98	1.8	723	1.95	2.4	471	0.65	833	0.76	115.3	152.2	13.0		
	#7	28.9	1.6	2.33	1.8	405	1.14	2.4	199	0.49	452	0.77	91.5	118.1	9.6		
	#8	25.9	1.6	1.49	1.8	638	0.52	2.4	223	0.35	691	0.70	131.2	187.9	19.1		
	#9	79.0	1.6	4.25	1.8	1036	6.45	2.4	1573	1.52	1406	0.76	112.3	148.2	12.6		
	#10	40.8	1.6	2.91	1.8	673	1.52	2.4	350	0.52	755	0.74	102.5	137.9	12.3	150.9	7.7

Amount of helium is given in nano-cubic-cm in standard temperature and pressure

Amount of radioactive elements are given in nanograms

eU (effective uranium concentration) is calculated as [U µg/g] + 0.235 × [Th µg/g]

Ejection correct (Ft): correction factor for alpha-ejection (according Hourigan et al. 2005)

Uncertainties of helium and the radioactive element contents are given as 1 sigma, in relative error %

Uncertainty of the single grain age is given as 2 sigma in Ma and it includes both the analytical uncertainty and the estimated uncertainty of the Ft

AFT data from within the Harz Mountains are strikingly similar regardless of elevation, lithology, or location. The low variability in ages, long mean track lengths and narrow track length distributions call for rapid cooling of the exhuming Harz block through the apatite partial annealing zone (PAZ; 50–140 °C; Gleadow et al. 1983, Gleadow et al. 1986; Green et al. 1989) in Late Cretaceous time. The same holds for the Kyffhäuser block further south (Fig. 3). This is supported by similar mean AHe ages scattering around the K–T boundary (69–63 Ma), indicating that exhumation continued into the Paleogene. Thermal modelling of the Brocken and Ramberg plutons as well as the Kyffhäuser block corroborates onset of exhumation around 90 Ma, rapid cooling between 85 and 65 Ma, and continued exhumation into the Paleogene (Fig. 6A–C). Assuming a geothermal gradient of 30 °C/km exhumation rates for the Brocken pluton can be estimated at > 0.5 km/Myr.

At the southern and western rim of the Harz Mountains, significantly older AFT ages (144–110 Ma) and more complex track length distributions are associated with younger AHe ages (76–58 Ma; Fig. 3), implying a more complex burial-exhumation history, which is supported by thermal modelling. Close to the westernmost edge of the Harz Mountains an Early Triassic sandstone sample (V-124) indicates cooling already in Early Cretaceous time, followed by a pulse of accelerated cooling at ~ 80 Ma (Fig. 6D). Early Cretaceous slow cooling may be generally assigned to thermal relaxation after periods of extension and increased heat flow in the Jurassic that affected a significant part of continental Europe (Littke et al. 2008). South of the Harz Mountains, Early Triassic sandstones (V-126, V-205) suggest Late Jurassic to Early Cretaceous cooling followed by a phase of no cooling and/or heating in Late Cretaceous (Fig. 6E, F). This thermal perturbation is not as clearly constrained as the simple and fast cooling trends of the granite bodies of the Harz Mountains and the Kyffhäuser block, however, it deserves special attention because (i) the sense of the thermal anomaly is opposite to the general trend observed in the Harz Mountains and (ii) it is documented independently for two samples in similar tectono-stratigraphic position. We interpret the

Table 3 Apatite fission track results obtained on basement and Mesozoic samples from the Harz Mountains and surroundings

Sample	Cryst.	Spontaneous		Induced		Dosimeter		$P(\chi^2)$	Disp.	FT age[a]	MTL		s.d.	*n*	Dpar	Cl content
		RhoS	Ns	RhoI	Ni	RhoD	Nd	[%]		[Ma ± 1 s]	[µm ± s.e.]				[µm]	[wt %]
V-1	25	0.89	953	1.59	1712	0.66	6454	49	0.03	59.3 ± 2.7	13.60	0.19	1.54	63	2.02	
V-2	22	1.36	1172	2.23	1927	0.70	5252	65	0.02	68.7 ± 2.9	12.91	0.21	1.39	42	1.86	
V-13	22	1.80	955	1.86	985	0.69	5252	2	0.17	110.0 ± 7.1	12.78	0.26	2.05	60	2.16	
V-15	25	3.91	2356	3.39	2043	0.70	5252	0	0.21	132.0 ± 7.6	11.95	0.29	2.23	60	1.99	
V-122	25	2.69	1091	2.10	852	0.62	6013	82	0.00	127.8 ± 6.4	12.65	0.24	1.84	59	2.42	
V-124	25	2.37	833	1.92	674	0.63	5232	100	0.00	124.7 ± 6.9	12.71	0.25	1.96	60	2.41	
V-125	24	3.16	1104	2.20	768	0.63	6013	93	0.00	144.3 ± 7.4	12.01	0.21	1.64	60	2.38	
V-126	24	2.99	1163	2.30	896	0.62	6013	93	0.00	127.8 ± 6.2	11.90	0.26	2.01	61	2.55	
V-202	22	1.89	950	2.14	1079	0.67	5610	99	0.00	94.5 ± 4.6	13.95	0.18	1.37	60	2.36	
V-205	23	2.92	1066	2.44	890	0.61	5610	99	0.00	117.2 ± 5.8	11.94	0.21	1.63	59	2.09	
BR 268	20	3.58	470	8.00	1050	1.00	6901	10	0.13	77.4 ± 5.8	13.73	0.16	1.25	61		
BR 269 B	38	1.01	1040	2.28	2351	0.96	4199	87	0.00	79.0 ± 4.3	13.29	0.27	1.56	34		0.006–0.078
BR 270	40	0.74	788	1.74	1845	0.98	4199	97	0.00	79.7 ± 4.9	13.28	0.24	1.24	26		0.002–0.016
BR 272	40	1.06	1419	2.55	3427	1.00	4199	53	0.09	75.8 ± 3.9	12.69	0.26	1.20	22		0.004–0.014
BR 273	35	0.96	869	2.41	2359	1.02	4199	55	0.16	78.5 ± 4.3	13.38	0.37	1.37	14		0.001–0.021
BR 274	40	1.25	1932	2.81	4357	1.04	4199	95	0.00	81.7 ± 3.6	13.69	0.14	0.98	49		0.005–0.019
BR 275	29	1.07	594	2.46	1392	1.06	4199	100	0.00	79.9 ± 5.9	12.74	0.42	1.27	9		0.003–0.029
BR 277	40	1.44	1655	3.41	3999	1.08	4199	97	0.00	79.0 ± 3.3	13.01	0.13	1.02	57		0–0.005
BR 278	40	0.83	850	1.95	1995	1.10	4199	100	0.00	79.3 ± 4.3	12.54	0.31	1.28	17		0–0.094
BR 280	20	1.06	213	2.33	470	1.00	6911	100	0.00	80.2 ± 6.9						
BR 281 C	20	0.89	434	1.91	935	1.00	6913	99	0.00	82.1 ± 5.2						
BR 282	20	1.18	399	2.71	914	1.08	7457	93	0.01	82.9 ± 5.2	13.93	0.11	1.06	100		
BR 387	10	0.31	93	0.88	261	1.15	4199	100	0.00	77.3 ± 9.4						
HF 3-1	20	0.37	199	0.82	439	0.95	4076	100	0.00	81.0 ± 7.0	14.36	0.21	0.56	7		0.005–0.077
HF 4	20	0.30	180	0.70	425	0.98	4076	100	0.00	78.2 ± 7.1						0.006–0.078
HF 5	17	0.37	162	0.92	401	1.00	4076	100	0.00	75.8 ± 7.2	13.16	0.53	1.42	7		0.003–0.080
HF 6	20	1.28	409	3.08	986	1.01	4076	100	0.00	79.1 ± 4.8	14.11	0.16	1.17	53		0.004–0.016
B1-2	8	0.38	75	0.91	179	1.03	4076	98	0.00	81.1 ± 11.2	13.48	0.31	0.87	8		0.006–0.090
B2-1	20	0.42	274	1.04	678	1.05	4076	100	0.00	79.5 ± 5.8	14.27	0.23	0.87	14		0.005–0.077
B4-2	20	0.62	370	1.60	957	1.08	4076	100	0.00	78.4 ± 5.0						0.006–0.082
B5-1	20	0.67	403	1.72	1032	1.09	4076	100	0.00	80.3 ± 4.9	13.94	0.36	1.13	10		0.005–0.065
B7	8	0.36	78	0.94	207	1.12	4076	100	0.00	79.7 ± 10.7						0.009–0.080
B9	19	0.40	300	1.12	836	1.14	4076	100	0.00	77.0 ± 5.3	14.28	0.27	0.71	7		0.009–0.081
OK 4	25	0.48	355	1.22	899	1.23	8542	92	0.00	82.0 ± 5.2	14.3	0.38	1.36	14		
OK 13	4	0.34	39	0.88	100	1.16	6435	96	0.00	76.2 ± 14.4						
GB	25	0.65	409	1.86	1173	1.23	8542	1	0.24	73.0 ± 5.6	13.72	0.24	1.71	50		

Track densities (Rho) are as measured (x10^6 tr/cm^2); number of tracks counted (*N*) shown in brackets

P (χ^2) probability obtaining Chi-square value for *n* degree of freedom (where *n* no. crystals-1)

Cryst number of dated apatite crystals, *Disp* dispersion, according to Galbraith and Laslett (1993), *MTL* mean horizontal confined track length

[a]Central ages

minor positive thermal anomalies between approx. 90 and 60 Ma as reflecting the accumulation and thermal blanketing effect of detritus (e.g. Luszczak et al. 2017) removed from the exhuming Harz Mountains. Transport of eroded material from the uplifting Harz towards south is a plausible scenario implying that the southern margin of the present day Harz Mountains experienced sediment accumulation and subsidence similar to the still preserved SCB in the north but with likely lower amplitude. Such interpretation would mirror a kind of 'retro-thrustblock' basin, which is common in cases of large fold and thrust belts (i.e. retro-foreland basins; Naylor and Sinclair 2008) but has not yet been described for small thrust blocks in Central Europe. The intermittently stored material at the southern rim of the Harz Mountains

Table 4 Apatite (U–Th)/He results obtained on basement and Mesozoic samples from the Harz Mountains

Sample	Aliq.	He		U238			Th232			Th/U	Sm			eU*	Ejection	Uncorr.	Ft-Corr.	2σ	Sample unweighted aver. ± 1 s.e.	
		Vol.	1σ	Mass	1	Conc.	Mass	1	Conc.		Mass	1σ	Conc.		Correct.	He-age	He-age			
		[ncc]	[%]	[ng]	[%]	[µg/g]	[ng]	[%]	[µg/g]	ratio	[ng]	[%]	[µg/g]	[µg/g]	(Ft)	[Ma]	[Ma]	[Ma]	[Ma]	[Ma]
EY40-4	#2	0.351	1.1	0.047	2.5	38	0.062	2.7	46	1.33	0.54	12.7	221	50	0.67	43.9	66.0	1.5		
	#3	2.989	0.4	0.287	1.8	28	0.497	2.4	48	1.73	2.85	9.1	278	41	0.79	57.5	72.7	1.1		
	#4	0.442	1.0	0.055	2.3	35	0.070	2.7	41	1.26	0.36	12.7	231	46	0.70	48.7	69.2	1.4		
	#5	1.354	0.6	0.151	1.9	34	0.162	2.5	35	1.07	0.92	12.7	206	43	0.78	56.6	72.9	1.2		
	#6	0.778	0.8	0.094	2.0	33	0.167	2.5	56	1.77	0.67	12.9	236	48	0.72	46.2	63.9	1.1		
	#7	0.762	0.8	0.079	2.1	29	0.113	2.6	39	1.43	0.69	6.0	252	40	0.72	56.6	78.3	1.4		
	#8	0.504	0.9	0.079	2.1	34	0.133	2.5	55	1.68	0.58	6.3	252	49	0.70	36.1	51.5	0.9	67.8	3.3
EY40-7	#1	0.208	1.5	0.021	3.8	7	0.047	2.8	15	2.31	2.09	4.7	750	14	0.74	35.2	47.5	1.3		
	#2	0.238	1.5	0.031	2.8	32	0.028	3.2	23	0.91	0.73	4.6	783	42	0.61	45.1	74.1	1.9		
	#4	0.424	1.0	0.038	2.6	15	0.051	2.8	18	1.36	2.04	4.4	824	23	0.68	52.6	76.9	1.6		
	#5	0.553	0.9	0.054	3.1	30	0.039	3.1	19	0.73	1.06	2.7	603	38	0.76	63.6	84.0	2.0		
	#6	0.952	0.7	0.092	2.0	16	0.138	2.5	23	1.49	3.86	2.8	664	25	0.78	50.2	64.0	1.0		
	#7	0.669	0.9	0.065	2.1	14	0.055	2.8	11	0.85	3.00	3.1	668	20	0.78	54.0	69.3	1.2		
	#8	0.701	0.8	0.041	2.5	8	0.253	2.5	48	6.25	4.64	3.5	905	24	0.75	41.7	55.5	1.0	67.3	4.8
EY40-9	#1	0.135	1.8	0.018	5.8	11	0.038	3.0	20	2.09	1.69	10.5	1037	21	0.65	27.0	42.3	2.0		
	#2	0.350	1.1	0.033	3.2	18	0.091	2.6	47	2.76	2.21	10.3	1237	36	0.66	39.7	65.2	2.1		
	#4	0.530	0.9	0.054	2.2	30	0.045	2.9	22	0.83	1.67	2.7	940	40	0.68	55.7	81.8	1.5	63.1	11.4
EY40-10	#2	0.475	0.9	0.059	2.5	20	0.040	3.0	11	0.68	2.11	6.5	728	26	0.79	45.9	60.9	1.3		
	#3	2.825	0.5	0.091	2.1	14	0.711	2.4	109	7.83	6.46	6.6	998	46	0.79	74.6	97.9	1.8		
	#4	0.373	1.1	0.038	2.9	15	0.029	3.3	9	0.77	2.49	12.7	500	20	0.77	47.2	64.3	2.7		
	#5	0.309	1.2	0.037	2.9	9	0.046	2.9	10	1.24	3.76	12.8	483	14	0.82	32.2	41.4	2.1		
	#7	1.289	0.6	0.072	2.1	16	0.128	2.5	26	1.77	4.95	12.8	539	25	0.82	74.1	95.0	3.5		
	#8	0.279	1.2	0.030	3.5	13	0.033	3.2	11	1.10	2.33	12.7	510	18	0.75	40.7	56.8	2.6		
	#9	0.401	1.1	0.042	2.7	13	0.035	3.1	9	0.83	3.23	12.7	509	18	0.77	42.9	56.8	2.6	67.6	7.9
V-2	#2	0.527	1.1	0.068	5.5	123	0.043	3.3	77	0.63	0.19	2.0	336	144	0.73	54.8	75.5	9.4		
	#3	0.148	1.6	0.006	73.5	33	0.069	2.9	346	10.64	0.05	3.4	269	121	0.64	52.6	81.9	33.7		
	#4	0.146	1.7	0.023	16.4	61	0.084	2.8	219	3.61	0.10	2.5	268	117	0.56	27.5	48.8	10.6	68.7	10.1
V-13	#1	0.243	2.2	0.051	2.0	96	0.008	4.5	16	0.17	0.05	9.7	91	100	0.58	37.8	64.8	8.9		
	#2	0.023	4.8	0.003	15.4	5	0.007	5.1	10	2.16	0.02	9.6	28	7	0.62	40.1	65.1	15.9		
	#3	0.128	2.4	0.019	3.0	24	0.058	2.7	74	3.06	0.38	9.4	483	45	0.66	29.3	44.2	5.2	58.0	6.9
V-122	#1	1.432	1.7	0.198	1.8	55	0.118	2.5	33	0.60	1.99	5.2	550	66	0.72	48.7	67.4	6.4		
	#3	0.604	1.9	0.075	1.9	29	0.012	3.9	5	0.16	0.35	5.2	138	31	0.64	61.8	96.2	11.4	81.8	20.4

Table 4 (continued)

Sample	Aliq.	He		U238			Th232			Th/U	Sm			eU*	Ejection	Uncorr.	Ft-Corr.	2σ	Sample unweighted aver. ± 1 s.e.	
		Vol.	1σ	Mass	1	Conc.	Mass	1	Conc.		Mass	1σ	Conc.		Correct.	He-age	He-age			
		[ncc]	[%]	[ng]	[%]	[μg/g]	[ng]	[%]	[μg/g]	ratio	[ng]	[%]	[μg/g]	[μg/g]	(Ft)	[Ma]	[Ma]	[Ma]	[Ma]	[Ma]
V-124	#2	0.583	1.8	0.092	1.9	28	0.003	9.0	1	0.03	0.40	10.5	122	29	0.67	50.2	74.6	8.2		
	#3	0.424	1.9	0.088	1.9	23	0.007	4.9	2	0.08	0.07	10.3	18	24	0.60	38.6	64.3	8.4		
	#4	0.161	2.4	0.020	3.0	2	0.016	3.5	2	0.78	0.43	10.3	53	3	0.71	48.9	68.8	7.7	69.2	3.0
V-125	#2	1.259	1.7	0.184	1.8	87	0.007	5.2	3	0.04	0.38	5.2	180	89	0.64	54.9	86.4	10.4		
	#3	0.779	1.8	0.132	1.9	68	0.045	2.8	24	0.34	0.97	5.4	504	77	0.66	42.8	65.1	7.4	75.8	15.1
V-126	#1	1.443	1.7	0.254	1.8	207	0.008	3.6	7	0.03	0.31	5.4	255	210	0.68	46.0	67.3	7.2		
	#2	0.750	1.8	0.112	1.9	89	0.008	3.6	6	0.07	0.28	5.3	223	92	0.76	53.2	70.1	6.2	68.7	2.0
V-205	#1	0.090	2.4	0.016	4.1	17	0.002	48.0	2	0.11	0.18	2.4	193	18	0.64	42.7	66.6	9.3		
	#2	0.093	2.3	0.013	4.5	8	0.002	60.7	1	0.13	1.25	2.4	741	12	0.71	32.1	45.3	5.1		
	#3	0.797	1.2	0.126	1.9	124	0.002	64.7	2	0.01	0.21	2.4	207	125	0.65	51.3	78.8	8.9		
	#4	1.101	1.2	0.149	1.8	106	0.004	2.5	3	0.03	0.31	2.4	219	108	0.66	59.4	89.8	9.9	70.1	9.5

Amount of helium is given in nano-cubic-cm in standard temperature and pressure

Amount of radioactive elements are given in nanograms

eU* (effective uranium concentration) is calculated as [U μg/g] + 0.235 × [Th μg/g] + 0.005 × [Sm μg/g]

Ejection correct (Ft) correction factor for alpha-ejection (according to Farley et al. 1996)

Uncertainties of helium and the radioactive element contents are given as 1 sigma. in relative error %

Uncertainty of the single grain age is given as 2 sigma in Ma and it includes both the analytical uncertainty and the estimated uncertainty of the Ft

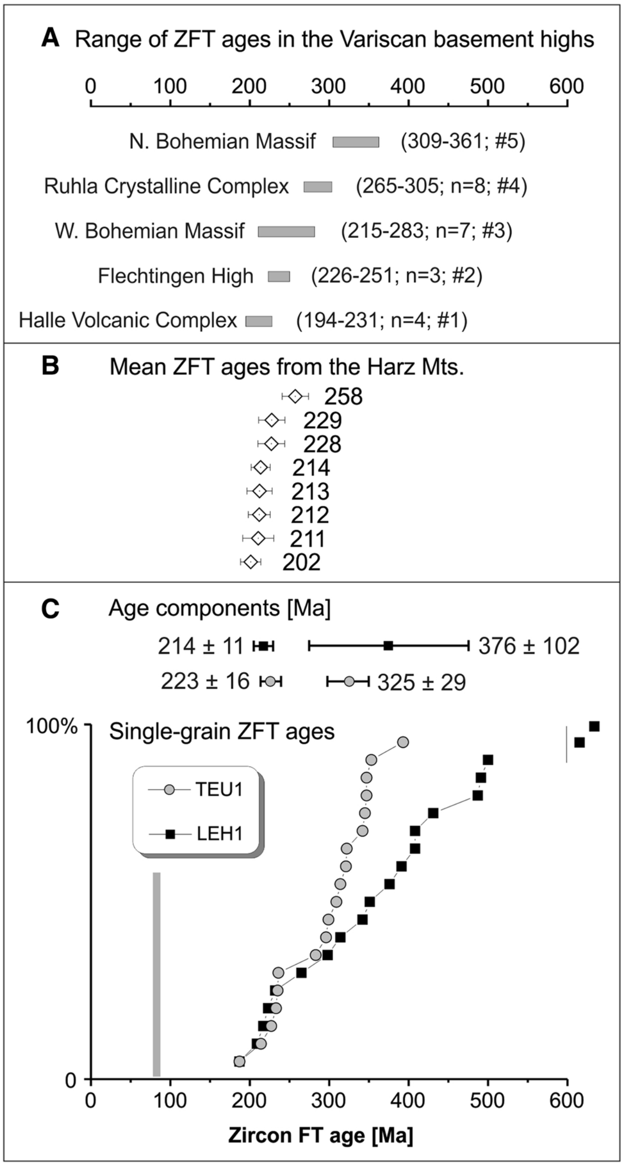

Fig. 4 Summary of zircon fission track (ZFT) data evaluation. **A** Compilation of mean ZFT ages obtained from Paleozoic basement highs and the Late Carboniferous Halle Volcanic Complex to the east of the Harz Mountains (#1—Jacobs and Breitkreuz 2003; #2—Fischer et al. 2012; #3—Hejl et al. 1997; #4—Thomson and Zeh 2000; #5—Migoń and Danišík 2012). **B** Sample mean ZFT ages from crystalline basement of the Harz Mountains. **C** cumulative frequency plot of detrital ZFT single-grain ages obtained from Late Cretaceous siliciclastic rocks of the Subhercynian Cretaceous Basin (vertical gray bar represents sedimentation age; *LEH1* Middle Coniacian, *TEU1* lowermost Campanian). Age component identification has been done using PopShare (Dunkl and Székely 2002) assuming two age components

was later removed following latest Cretaceous to Tertiary uplift (Fig. 6E, F).

The Brocken area with its high density of samples and range of methods used underlines the internal consistency of the thermochronological data. Moreover, the data closely match independent information derived from the adjacent basin fill to the north (SCB). The youngest ZHe age component (96–90 Ma, mean at 93.6 ± 2.1 Ma) slightly predates the phase of erosion of the Mesozoic cover of the Harz (86–82 Ma; von Eynatten et al. 2008), which in turn slightly predates the tight range of AFT mean ages (83–73 Ma), followed by distinctly younger AHe single-grain ages with sample means between 68 and 63 Ma (Fig. 5). These new data allow for a tightly constrained reconstruction of the timing of exhumation and erosion of the Harz Mountains. Initial exhumation and cooling of granitoid rocks buried as deep as the transition between the total resetting zone and the PRZ for ZHe occurred at around 96–90 Ma. This age matches (i) similar ZHe data from the Flechtingen High (~92 Ma; Fischer et al. 2012), (ii) initial thickness changes within Turonian hemipelagic sediments of the SCB (ca. 94–90 Ma; Voigt et al. 2006) and (iii) at a continental scale, the onset of compression in Central Europe at ca. 90 Ma due to the change in motion of Africa relative to Europe (Kley and Voigt 2008). Increasing uplift and emergence of the Harz

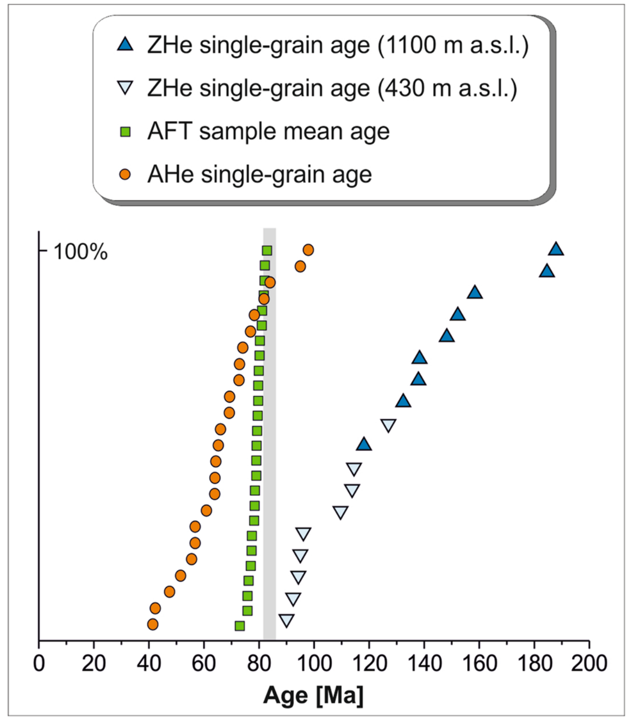

Fig. 5 Cumulative frequency plot of single-grain apatite and zircon (U–Th)/He ages (AHe and ZHe, respectively) and apatite fission-track (AFT) sample means, all obtained from the Brocken area. For ZHe data the samples representing the summit (EY40-9, 1105 m a.s.l.) and the valley (EY40-4, 432 m a.s.l.) are distinguished. The lower sample shows a pronounced asymmetry with five ZHe ages forming a tight cluster with a mean age of 93.6 ± 2.1 Ma (five crystals dated between 90.0 and 96.1 Ma). The grey bar indicates the timing (86–82 Ma) of removal of the Mesozoic cover of the Harz Mountains as inferred from the adjacent sedimentary basin fill (von Eynatten et al. 2008)

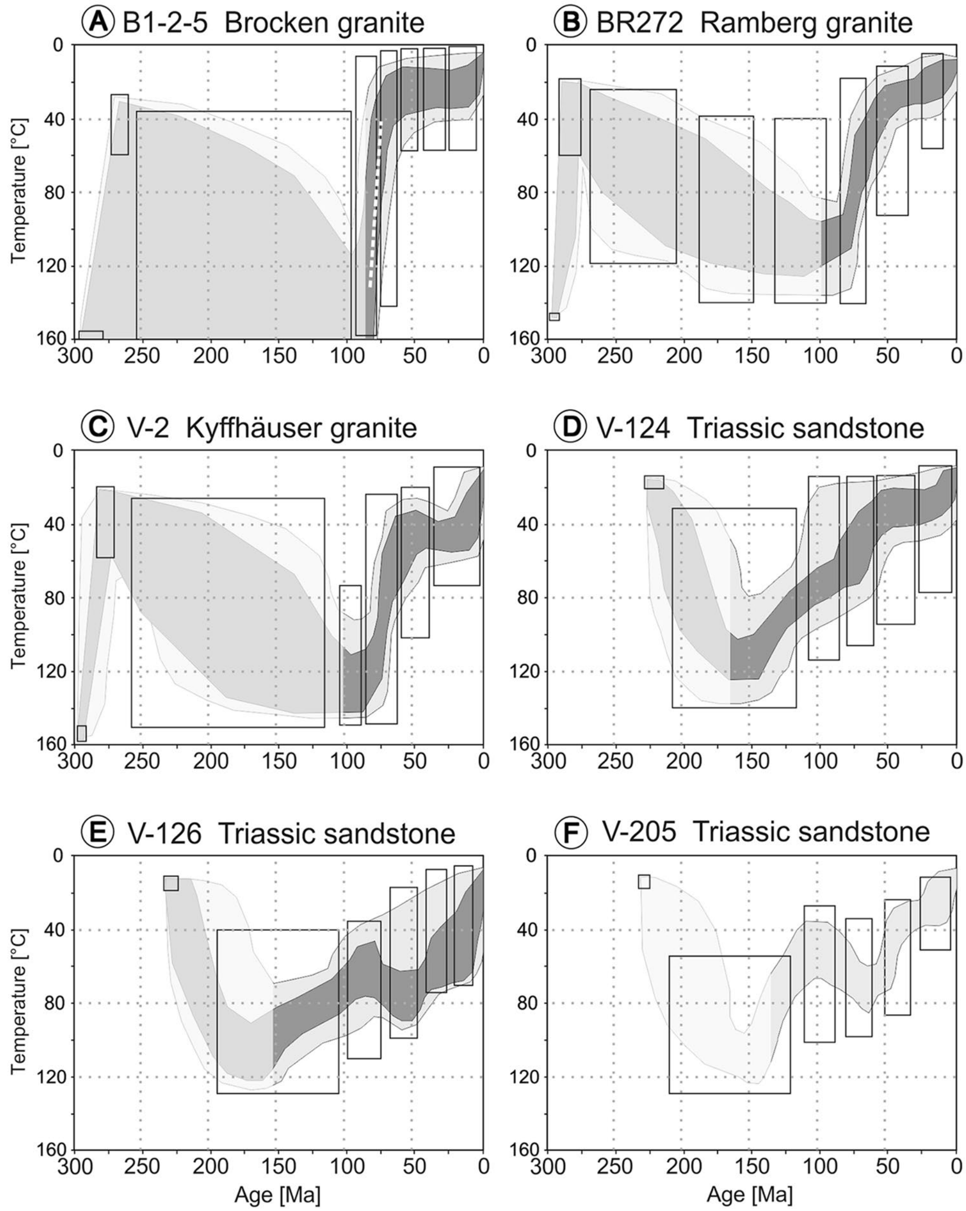

Fig. 6 Time-temperature plots showing results of thermal modelling. **A–C** Late Variscan plutons of the Brocken and the Ramberg within the Harz Mountains and the Kyffhäuser block, respectively. For the Brocken pluton three similar samples have been pooled (B1–2, B2–1, and B5–1; see Table 3). **D–F** Early Triassic sandstones from the western and southern rim of the Harz Mountains. Grey boxes represent the time–temperature constraints applied to the modelling runs allowing for unsupervised thermal paths, except for the initial post-metamorphic conditions, the age of sediment onlapping (basement samples) or age of sedimentation (Triassic samples), and the current annual mean temperature. Light grey belt is the envelope of acceptable fits, while dark grey marks the envelope of good fits. The pale fields to the left of each plot indicate the time–temperature ranges where the modelling results should not be considered because the thermochronological memory of the earlier part of the evolution has been erased by younger high temperature events. Stippled white line in (**A**) refers to exhumation rate of 0.5 km/Myr assuming geothermal gradient of 30 °C/km

Mountains then triggered the erosion of the Mesozoic cover, which started at 86–85 Ma and was largely completed by 83–82 Ma (von Eynatten et al. 2008). This was followed by erosion of Paleozoic rocks, which initially should exceed about 3–4 km in thickness because all AFT mean ages are younger than 83–82 Ma. Exhumation and erosion continued into the Paleogene, implying that final uplift and formation of the Harz Mountains including the last phase of peneplanation is a Cenozoic feature (e.g., König et al. 2011).

Assuming an average geothermal gradient of 30 °C/km, our partially to fully reset ZHe data (typically equivalent to temperatures of ~ 130–220 °C; Reiners et al. 2004; Guenthner et al. 2013, but might be lower in highly radiation-damaged grains, e.g. Johnson et al. 2017) imply burial and subsequent removal of at least 5 km of overburden from the present surface of the Harz since Cenomanian–Turonian time. AFT data suggest removal of > 3–4 km of Paleozoic rocks (= E_{PZ} in Fig. 7) after 83–82 Ma, i.e. after removal of the overlying Permo–Mesozoic sedimentary section. These numbers are consistent with a potential overburden of 5–10 km inferred from geologic data, based on (i) the intrusion depth of the Brocken pluton, which is estimated at 3–7 km based on isotopic evidence and phase relations in contact metamorphic rocks (Baumann et al. 1991; Franz et al. 1997), (ii) ~ 2 km Upper Permian (Zechstein) and Triassic sedimentary rocks (e.g., Voigt et al. 2006; McCann 2008), and (iii) Jurassic to Cenomanian sedimentary rocks, which are highly variable in thickness ranging from almost zero to ~ 1.5 km (Fig. 7; E_{PZ}, E_{PT}, and E_{JC}, respectively). The intrusion depth, however, is not a reliable estimate of E_{PZ},

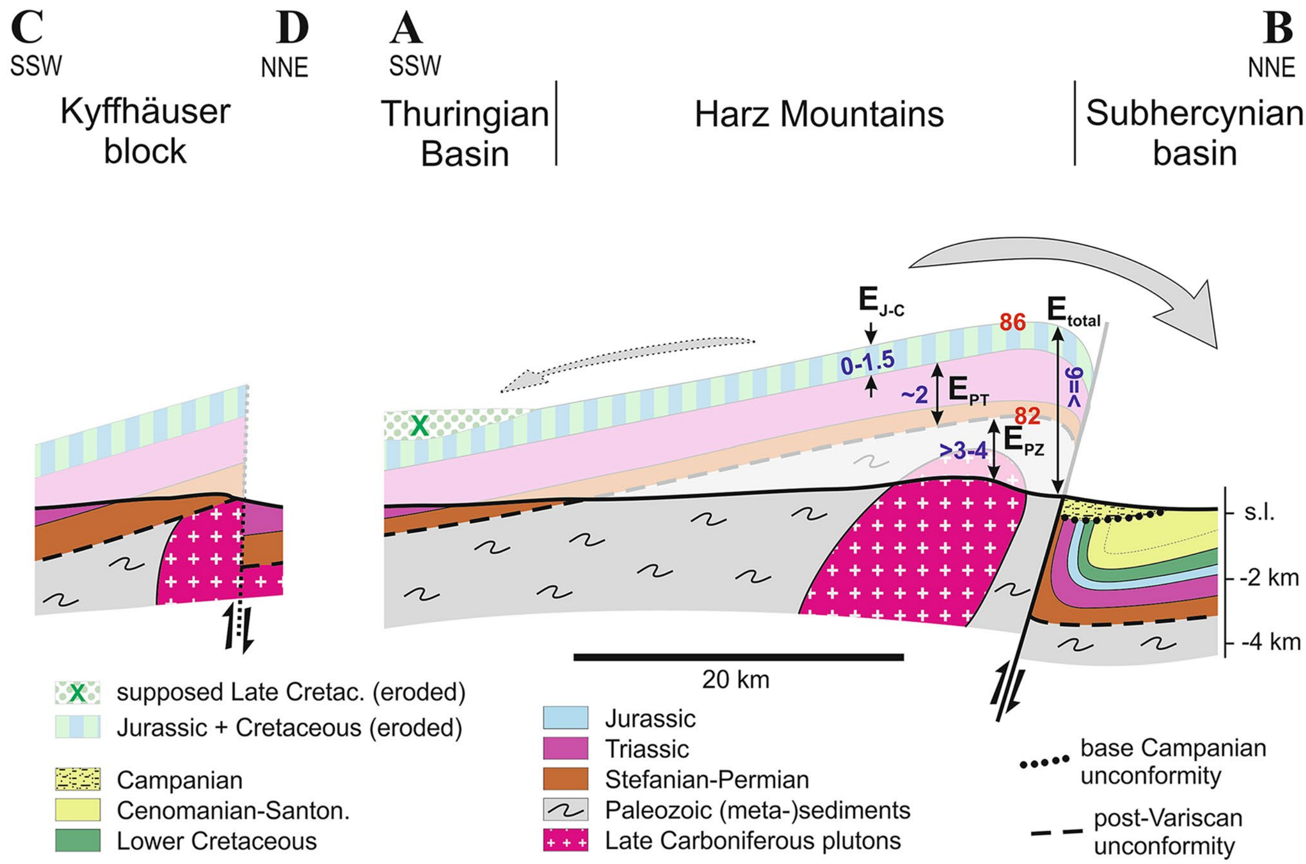

Fig. 7 Cross section of the Harz Mountains and the adjacent basin parts to the north and south including position and inferred thickness of the strata removed in Late Cretaceous time (modified after Kley et al. 2008; vertical exaggeration = 2). For tentative position of cross sections see Fig. 2. E_{total} total thickness of the removed basement and the Permo–Mesozoic strata, E_{PZ} thickness of eroded Paleozoic rocks, E_{PT} thickness of eroded Permo–Triassic strata, $E_{J\text{–}C}$ thickness of eroded Jurassic-Cretaceous strata. Green X indicates position of possible Late Cretaceous sediment accumulation south of the Harz Mountains which has been later eroded. Blue numbers show inferred thicknesses for individual *E* values and red numbers indicate the timing at which the erosion of the different levels started or was completed, as discussed in the text

because the thickness of Paleozoic metasedimentary rocks removed following pluton emplacement, and before Late Permian (Zechstein) transgression is essentially unknown, as is the amount of granite already removed from the presently exposed surface of the Brocken pluton. The entire amount of overburden removed can thus be estimated at $E_{\text{total}} \geq 6$ km, the majority of which has occurred in Santonian–Campanian time. The removal (i.e. erosive exhumation) rate of the Mesozoic cover has been estimated at ~ 1 km/Myr (von Eynatten et al. 2008), which roughly equals the rates predicted from thermal modelling. However, the latter rates appear somewhat lower, likely because of the uncertainties inherent in the good and acceptable fit paths of the modelling and/or their integration over longer time spans compared to the short phase of erosion of the Permo–Mesozoic cover (2–4 Myr).

In contrast to the fully reset and/or partially reset ages recorded by the lower temperature thermochronometers, the ZFT data from Upper Cretaceous sandstone of the SCB reveal detrital ages that show distinct differences between the middle Coniacian and lowermost Campanian samples (Fig. 4C). These contrasting detrital signatures are in-line with major facies and provenance changes that occurred within the Santonian and are related to the erosion of the Mesozoic cover of the exhuming Harz (see above). Both samples reveal a distinct Late Triassic age component (214 and 223 Ma), however, the stratigraphically younger sample (TEU1) shows a distinct Variscan age component (325 ± 29 Ma), while in the older sample (LEH1) Paleozoic single-crystal ZFT ages show a very broad distribution with poorly defined age components (Fig. 4C). The Variscan ages most likely reflect recycling of Early Triassic clastics (i.e. Buntsandstein; Köppen and Carter 2000) and/or Variscan basement rocks not affected by Permo–Triassic burial. Recycling of Buntsandstein at about the Santonian–Campanian transition is strongly supported by heavy mineral associations and mineral chemistry (von Eynatten et al. 2008). The Late Triassic ZFT ages likely reflect erosion of Variscan basement rocks and Late Paleozoic volcanic rocks affected by Permo–Triassic burial as described above (Fig. 4A, B). Similar ages may also be explained by recycling of Late Triassic (Keuper) clastic rocks (Köppen and Carter 2000; Tatzel et al. 2017).

Conclusions

The Harz Mountains and the adjacent Subhercynian Cretaceous Basin constitute one of the most prominent surface expressions of Late Cretaceous uplift and inversion structures in Central Europe. The combination of multi-method thermochronology of Harz basement rocks and Early Triassic sedimentary rocks of the western and southern rim of the Harz Mountains and provenance analysis of the Subhercynian Cretaceous Basin allow for a detailed reconstruction of the timing and rates of exhumation and erosion of the Harz Mountains. Shortening and exhumation initiated at around 90 Ma, significant uplift and onset of rapid erosion of the Mesozoic cover is dated at 86–85 Ma and was largely completed by 83–82 Ma. This was followed by erosion of at least 3–4 km of Paleozoic rocks, which continued into the Paleogene. The thickness of the removed overburden amounts to at least 6 km, with the majority of erosion occurring in Santonian to Campanian time at average rates of 0.5–1 km/Myr. The southern and western rim of the Harz Mountains were exhumed at a much slower rate over a longer period of time, and the southern margin may record a phase of Late Cretaceous syntectonic sediment accumulation and reburial, similar to the Subhercynian Cretaceous Basin in the north.

This case study serves as an excellent example of the benefits of integrated analysis of multi-method thermochronology with high stratigraphic resolution sedimentary provenance analysis to decipher the timing, amplitude, and rates of exhumation/uplift processes in convergent intraplate settings.

Acknowledgements We thank Björn Baresel, Eike-Matthias Bultmann, Katrina Kremer, Florian Wetzel and Jörn-Frederic Wotzlaw for supporting the (U–Th)/He analysis at University of Göttingen, Frank Hansen for mineral separation at Ruhr University Bochum, and Jonas Kley and Thomas Voigt for valuable discussions. Thorough reviews by Martin Danišík and an anonymous reviewer helped to improve the final manuscript.

References

Baumann A, Grauert B, Mecklenburg S, Vinx R (1991) Isotopic age determinations of crystalline rocks of the Upper Harz Mountains, Germany. Int J Earth Sci 80:669–690

Carlson WD, Donelick RA, Ketcham RA (1999) Variability of apatite fission-track annealing kinetics: I. Experimental results. Am Mineral 84:1213–1223

Danišík M, Migoń P, Kuhlemann J, Evans NJ, Dunkl I, Frisch W (2010) Thermochronological constraints on the long-term erosional history of the Karkonosze Mts, Central Europe. Geomorphology 117:78–89

Danišík M, Štěpančíková P, Evans NJ (2012) Constraining long-term denudation and faulting history in intraplate regions by multisystem thermochronology: An example of the Sudetic Marginal Fault (Bohemian Massif, central Europe). Tectonics 31:TC2003. https://doi.org/10.1029/2011tc003012

Danišík M, McInnes BIA, Kirkland CL, McDonald BJ, Evans NJ, Becker T (2017) Seeing is believing: visualization of He distribution in zircon and implications for thermal history reconstruction on single crystals. Sci Adv 3:e1601121

DEKORP-Basin Research Group (1999) Deep crustal structure of the northeast German Basin: new DEKORP BASIN 96 deep-profiling results. Geology 27:55–58

Donelick RA, O'Sullivan PB, Ketcham RA (2005) Apatite fission-track analysis. Rev Mineral Geochem 58:49–94

Dumitru TA (1993) A new computer automated microscope stage system for fission-track analysis. Nucl Tracks Radiat Meas 21:575–580

Dunkl I, Székely B (2002) Component analysis with visualization of fitting—PopShare, a Windows program for data analysis. Geochimica Cosmochimica Acta 66/15A, 201; http://www.sediment.uni-goettingen.de/staff/dunkl/software/popshare.html. Accessed 22 Jan 2019

Farley KA (2000) Helium diffusion from apatite: general behavior as illustrated by Durango fluorapatite. J Geophys Res 105:2903–2914

Farley KA, Wolf RA, Silver LT (1996) The effects of long alpha-stopping distances on (U–Th)/He ages. Geochim Cosmochim Acta 60:4223–4229

Fischer C, Dunkl I, von Eynatten H, Wijbrans JR, Gaupp R (2012) Products and timing of diagenetic processes in Upper Rotliegend sandstones from Bebertal (North German Basin, Parchim Formation, Flechtingen High, Germany). Geol Mag 149:827–840

Flick H (1986) The Hercynian Mountains—a postorogenic overthrusted massif? Naturwissenschaften 73:670–671

Franz L, Schuster AK, Strauss KW (1997) Basement Evolution in the Rhenohercynian Segment: discontinuous Exumation History of the Eckergneis Complex (Harz Mountains, Germany). Chem Erde 57:105–135

Franzke HJ, Voigt T, von Eynatten H, Brix MR, Burmester G (2004) Geometrie und Kinematik der Harznordrandstörung, erläutert an Profilen aus dem Gebiet von Blankenburg. Geowiss Mitt Thüringen 11:39–62

Franzke HJ, Müller R, Voigt T, von Eynatten H (2007) Paleo-Stress Paths in the Harz Mountains and surrounding areas (Germany) between Triassic and Upper Cretaceous. Z Geol Wiss 35:141–156

Galbraith RF (1981) On statistical models for fission track counts. Math Geol 13:471–471

Galbraith RF, Laslett GM (1993) Statistical models for mixed fission track ages. Nucl Tracks Radiat Meas 21:459–470

Gleadow AJW (1981) Fission track dating methods: what are the real alternatives? Nucl Tracks 5:3–14

Gleadow AJW, Hurford AJ, Quaife RD (1976) Fission track dating of zircon: improved etching techniques. Earth Planet Res Lett 33:273–276

Gleadow AJW, Duddy IR, Lovering JF (1983) Fission track analysis: a new tool for the evaluation of thermal histories and hydrocarbon potential. Aust Petrol Explor Assoc J 23:93–102

Gleadow AJW, Duddy IR, Green PF, Hegarty KA (1986) Fission track lengths in the apatite annealing zone and the interpretation of mixed ages. Earth Planet Sci Lett 78:245–254

Green PF (1981) 'Track-in track' length measurements in annealed apatites. Nucl Tracks 5:12–18

Green PF, Duddy IR, Laslett GM, Hegarty KA, Gleadow AJW, Lovering JF (1989) Thermal annealing of fission tracks in apatite 4. Quantitative modelling techniques and extension to geological timescales. Chem Geol Isot Geosci Sect 79:155–182

Guenthner WR, Reiners PW, Ketcham RA, Nasdala L, Giester G (2013) Helium diffusion in natural zircon: radiation damage, anisotropy, and the interpretation of zircon (U–Th)/He thermochronology. Am J Sci 313:145–198

Hejl E, Coyle D, Lal N, van den Haute P, Wagner GA (1997) Fission-track dating of the western border of the Bohemian massif: thermochronology and tectonic implications. Int J Earth Sci 86:210–219

Hourigan JK, Reiners PW, Brandon MT (2005) U-Th zonation-dependent alpha-ejection in (U-Th)/He chronometry. Geochimica et Cosmochimica Acta 69(13):3349–3365

Hurford AJ (1990) Standardization of fission track dating calibration: recommendation by the Fission Track Working Group of the IUGS Subcommission on Geochronology. Chem Geol 80:171–178

Hurford AJ, Green PF (1983) The age calibration of fission-track dating. Isot Geosci 1:285–317

Jacobs J, Breitkreuz C (2003) Zircon and apatite fission-track thermochronology of Late Carboniferous volcanic rocks of the NE German Basin. Int J Earth Sci 92:165–172

Johnson JE, Flowers RM, Baird GB, Mahan KH (2017) "Inverted" zircon and apatite (U–Th)/He dates from the Front Range, Colorado: high-damage zircon as a low-temperature (< 50°C) thermochronometer. Earth Planet Sci Lett 466:80–90

Karg H, Carter A, Brix MR, Littke R (2005) Late- and post-Variscan cooling and exhumation history of the northern Rhenish massif and the southern Ruhr Basin: new constraints from fission-track analysis. Int J Earth Sci 94:180–192

Ketcham R (2005) Forward and inverse modeling of low-temperature thermochronometry data. Rev Mineral Geochem 58:275–314

Ketcham RA, Carter A, Donelick RA, Barbarand J, Hurford AJ (2007) Improved modeling of fission track annealing in apatite. Am Mineral 92:799–810

Kley J, Voigt T (2008) Late Cretaceous intraplate thrusting in central Europe: effect of Africa–Iberia–Europe convergence, not Alpine collision. Geology 36:839–842

Kley J, Franzke HJ, Jähne F, Krawczyk C, Lohr T, Reicherter K, Scheck-Wenderoth M, Sippel J, Tanner D, van Gent H (2008) Strain and Stress. In: Littke R, Bayer U, Gajewski D, Nelskamp (eds) Dynamics of complex intracontinental basins—the Central European Basin system. Springer, Berlin, pp 97–124

Kockel F (2003) Inversion structures in Central Europe—expressions and reasons, an open discussion. Neth J Geosci 82:367–382

König W, Köthe A, Ritz I (2011) Die marine Beeinflussung der Subherzynen Senke und der Mittelharzhochfläche im Oligozän—Biostratigraphische und sedimentpetrographische Analysen tertiärer Sandvorkommen. Z Geol Wiss 39:387–431

Köppen A, Carter A (2000) Constraints on provenance of the central European Triassic using detrital zircon fission track data. Palaeogeogr Palaeoclimatol Palaeoecol 161:193–204

Littke R, Bayer U, Gajewski D, Nelskamp S (2008) Dynamics of complex intracontinental basins—the Central European Basin system. Springer, Berlin, p 519

Łuszczak K, Persano C, Braun J, Stuart FM (2017) How crustal thermal properties influence the amount of denudation derived from low-temperature thermochronometry. Geology 45:779–782

Marotta AM, Bayer U, Scheck M, Thybo H (2001) The stress field below the NE German basin: Effects induced by the Alpine collision. Geophys J Int 144:F8–F12. https://doi.org/10.1046/j.1365-246x.2001.00373.x

McCann T (ed) (2008) The geology of central Europe. Volume 2: Mesozoic and Cenozoic. Geological Society, London

Migoń P, Danišík M (2012) Erosional history of the Karkonosze Granite Massif—constraints from adjacent sedimentary basins and thermochronology. Geol Q 56:441–456

Naylor M, Sinclair HD (2008) Pro- vs. retro-foreland basins. Basin Res 20:285–303

Reiners PW, Spell TL, Nicolescu S, Zanetti KA (2004) Zircon (U–Th)/He thermochronometry: he diffusion and comparisons with $^{40}Ar/^{39}Ar$ dating. Geochim Cosmochim Acta 68:1857–1887

Stackebrandt W, Franzke HJ (1989) Alpidic reactivation of the Variscan consolidated lithosphere: the activity of some fracture zones in central Europe. Z Geol Wiss 7:699–712

Tanner DC, Krawczyk CM (2017) Restoration of the Cretaceous uplift of the Harz Mountains, North Germany: evidence for the geometry of a thick-skinned thrust. Int J Earth Sci 106:2963–2972

Tatzel M, Dunkl I, von Eynatten H (2017) Provenance of Paleo-Rhine sediments from zircon thermochronology, geochemistry, U/Pb dating, and heavy mineral assemblages. Basin Res 29(suppl 1):396–417

Thomson SN, Zeh A (2000) Fission-track thermochronology of the Ruhla Crystalline Complex: new constraints on the post-Variscan thermal evolution of the NW Saxo-Bohemian Massif. Tectonophysics 324:17–35

Thomson SN, Brix MR, Carter A (1997) Late Cretaceous denudation of the Harz Massif assessed by apatite fission-track analysis. Schr Dtsch Geol Ges 2:115 **(abstract)**

Voigt T, von Eynatten H, Franzke HJ (2004) Late Cretaceous unconformities in the Subhercynian Cretaceous Basin (Germany). Acta Geol Pol 54:765–765

Voigt T, Wiese F, von Eynatten H, Franzke HJ, Gaupp R (2006) Fazies evolution of syntectonic Upper Cretaceous deposits in the Subhercynian Cretaceous Basin and adjoining areas (Germany). Z Dtsch Ges Geowiss 157:203–244

Voigt T, von Eynatten H, Kley J (2009) Kommentar zu "Nördliche Harzrandstörung: diskussionsbeiträge zu Tiefenstruktur, Zeitlichkeit und Kinematik". Z Dtsch Ges Geowiss 160(1):93–99

von Eynatten H, Voigt T, Meier A, Franzke HJ, Gaupp R (2008) Provenance of Cretaceous clastics in the Subhercynian Basin: constraints to exhumation of the Harz Mountains and timing of inversion tectonics in Central Europe. Int J Earth Sci 97(6):1315–1330

Ziegler PA (1987) Late Cretaceous and Cenozoic intra-plate compressional deformations in the Alpine foreland—a geodynamic model. Tectonophysics 137(1–4):389–420

Ziegler PA (1990) Geological Atlas of Western and Central Europe, 2nd edn. Shell Internationale Petroleum Mij. BV and Geological Society of London (London), pp 1–239

Ziegler PA, Cloetingh SAPL, van Wees JD (1995) Dynamics of intraplate compressional deformation: the Alpine foreland and other examples. Tectonophysics 252:7–59